To be published in Optics Letters:

Title: Optimization of Brillouin instantaneous frequency measurement using convolutional neura
Authors: Xiuting Zou,Shaofu Xu,Shujing LI,Jianping Chen,Weiwen Zou
Accepted: 21 October 19
Posted 24 October 19
Doc. ID: 375257

Optimization of Brillouin instantaneous frequency measurement using convolutional neural networks

XIUTING ZOU, SHAOFU XU, SHUJING LI, JIANPING CHEN, WEIWEN ZOU*

State Key Laboratory of Advanced Optical Communication Systems and Networks, Intelligent Microwave Lightwave Integration Innovation Center (iMLic), Department of Electronic Engineering, Shanghai Jiao Tong University, Shanghai 200240, China

**Correspondence to: wzou@sjtu.edu.cn.*

Received XX Month XXXX; revised XX Month, XXXX; accepted XX Month XXXX; posted XX Month XXXX (Doc. ID XXXXX); published XX Month XXXX

Brillouin instantaneous frequency measurement (B-IFM) is used to measure instantaneous frequencies of an arbitrary signal with high frequency and broad bandwidth. However, the instantaneous frequencies measured using the B-IFM system always suffer from errors due to system defects. To address this, we adopt a convolutional neural network (CNN), which establishes a function mapping between the measured and nominal instantaneous frequencies to obtain more accurate instantaneous frequency, thus, improving the frequency resolution, system sensitivity and dynamic range of the B-IFM. Using the proposed CNN-optimized B-IFM system, the average maximum and root mean square (RMS) errors between the optimized and nominal instantaneous frequencies are less than 26.3 MHz and 15.5 MHz, which is reduced from up to 105.8 MHz and 57.0 MHz. The system sensitivity is increased from 12.1dBm to 7.8 dBm for the 100-MHz frequency error and the dynamic range is larger.

OCIS codes: (070.4790) Spectrum analysis; (190.0190) Nonlinear optics; (200.4260) Neural networks

Owing to its merits, including ultra-wideband operation, good stability, and anti-interference properties, Instantaneous frequency measurement (IFM) based on microwave photonics [1-3] has become a powerful tool for the instantaneous detection and analysis of frequencies of unknown microwave signals. In [4], we present a Brillouin IFM (B-IFM) approach for broadband microwave signals. This approach takes use of the principle of frequency-to-power mapping based on stimulated Brillouin scattering (SBS) in an optical fiber. Nevertheless, because of system defects caused by various issues, such as non-ideal modulators, imperfect polarization states of lightwaves, and non-negligible loss of optical fibers, the instantaneous frequency of an unknown signal measured using the B-IFM system always deviates (by about 100.0 MHz) from the nominal value. Decision making based on such large frequency deviations in the fields of electromagnetic defense and counterintelligence, electronic warfare, and radar detection, could have serious and even irrevocable negative consequences. Hence, a feasible and effective method is required to improve the accuracy of the B-IFM approach. In recent years, the ability of convolutional neural networks (CNNs) to effectively extract critical features from data as well as to approximate arbitrary functions has been well-researched [5, 6]. And CNNs have been universally applied in computer vision [7], medical diagnosis [8], and other fields to remarkably improve the performance of existing approaches and/or provide an effective means to solve some challenging tasks that were left unsolved before them. Furthermore, in the field of photonics, CNNs have proved invaluable in improving optical system design and hardware as well as data processing and analysis [9, 10]. Most recently, the defects in a photonic analog-to-digital conversion (PADC) system were rectified using a CNN, effectively improving its performance [10].

In this study, we present a CNN-optimized B-IFM approach wherein a CNN is used to enhance the frequency accuracy of the original B-IFM system and improve the system sensitivity, and the dynamic range without changing its design or hardware. Through convolution, max pooling, and nonlinear activation operations, the proposed CNN establishes complex function mapping between the measured and nominal instantaneous frequencies. The instantaneous frequency measured by the B-IFM system is input into the CNN; then, the network outputs the optimized instantaneous frequency, which is closer to the nominal one than the originally measured value. To verify the feasibility of our proposed CNN-optimized B-IFM system, we test it with five types of unknown broadband signals, namely linear frequency modulated signal with up slope [LFM (up-chirp)], linear frequency modulated signal with down slope [LFM (down-chirp)], nonlinear frequency modulated (NLFM) signal, binary frequency-shift keying (BFSK) signal, and Costas frequency modulated pulses. Based on our evaluation results, when the power of the unknown broadband microwave signals is 13.01 dBm, the average maximum and root mean square (RMS) errors between the optimized and nominal instantaneous frequencies reduced to less

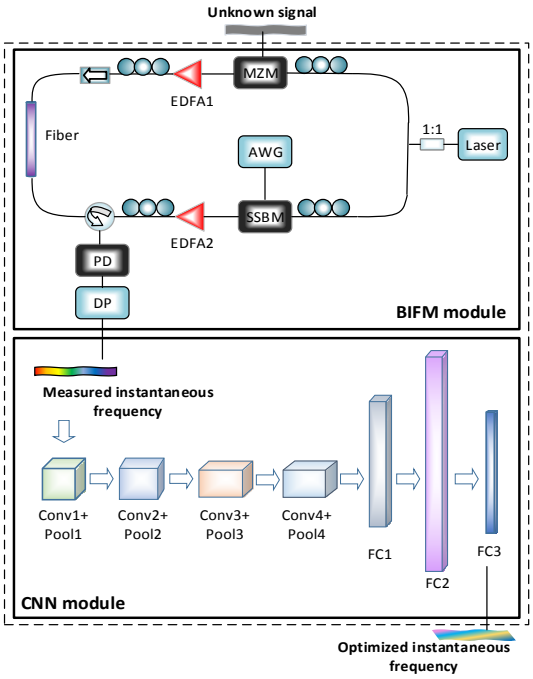

Fig.1. Design and experimental setup of the CNN-optimized B-IFM system. AWG: arbitrary waveform generator. SSBM: single sideband modulator. MZM: Mach-Zehnder modulator. EDFA: erbium-doped fiber amplifier. PD: photo-detector. DP: digital processing Conv1–Conv4, Pool1–Pool4, and FC1–FC3 refer to the convolutional, pooling, and fully connected layers, respectively.

than 26.3 MHz and 15.5 MHz, which were originally as high as 105.8 MHz and 57.0 MHz, respectively. In addition, we used the Costas frequency modulated signals to be measured to test the system sensitivity and dynamic range of our B-IFM system. By the optimization of the CNN, the system sensitivity is increased from 12.1 dBm to 7.8 dBm for the 100-MHz frequency error and the dynamic range becomes larger.

Figure 1 illustrates the design and experimental setup of the CNN-optimized B-IFM system. It includes two cascaded modules: the B-IFM module and CNN module. Using the B-IFM module, we measure the instantaneous frequency of an unknown broadband microwave signal in the same manner as described in [4]. In our original B-IFM system, a single sideband modulator (SSBM) loads a nonlinear frequency sweeping signal onto the pump lightwave. Bias drift in the SSBM can cause ineffective carrier suppression, which introduces defects in the SBS process [1, 11]. A Mach-Zehnder modulator (MZM) modulates an unknown signal or known LFM pulse signal onto a probe lightwave. Nevertheless, because of an inherently nonlinear electro-optic conversion response [12], both SSBM and MZM introduce nonlinear distortion into the pump and probe lightwaves, respectively. The probe and pump lightwaves enter into a dispersion compensating fiber (DCF) to produce SBS interaction. During this process, their non-ideal polarization state and loss in the DCF itself hamper the Brillouin gain of the probe lightwave. In addition, the power of the microwave signal also affects its Brillouin gain [4]. A photo-detector (PD) then converts the probe lightwave into electric voltage, which is digitized and recorded by an oscilloscope. A digital processing (DP) based on the principle of frequency-to-power mapping is employed after the PD to deduce the instantaneous frequency. Although we eliminate the influence of the power of the microwave signal by adopting two different sweeping pump lightwaves in [4], other defects as described above also introduce large errors in the obtained frequency values.

The CNN module is composed of four convolution layers (Conv1–Conv4), four max pooling layers (Pool1–Pool4), and three fully connected (FC1–FC3) layers. The windows' sizes of the convolution and max pooling layers are 1×3 and 1×2, respectively, in the 'SAME' padding manner. For Conv1 to Conv4, the numbers of feature maps are 16, 16, 32, and 32, respectively. The numbers of neurons in FC1–FC3 are 512, 1024, and the length of network input, respectively. Except for the output layer, i.e., the FC3 layer, other layers are followed by a rectified linear unit (ReLU), which performs the operation $\mathrm{ReLU}(x) = \max(0, x)$ [13]. The Pool1 to Pool4 are used to decrease the redundant information of input data and increase the training speed. We use L2 regularizer in the output layer to prevent overfitting [14].

Based on the universal approximation theorem for feedforward neural networks [6, 15], a CNN can develop the ability to approximate the complex function between the measured and nominal instantaneous frequencies through training. We can adopt a minimization algorithm to train the CNN, which reduces training loss *Loss(θ)* by adjusting the network trainable parameter θ:

$$\boldsymbol{Loss(\theta)} = \frac{1}{N}\left(\sum_{i=1}^{N}(Y_i^{\theta} - Y_i^{Ref})^2 + \lambda\sum_{i=1}^{N}\left|W_i^2\right|\right), \qquad \textbf{(1)}$$

where Y^{θ} is the network output, Y^{Ref} is the reference data (the nominal instantaneous frequencies), W denotes weights of the FC3 layer. N is the number of input dataset, and λ is the regularized parameter of the L2 regularizer. The network input includes the instantaneous frequencies measured by the B-IFM module. If the values for *Loss(θ)* decrease to a considerably small number after the training phase, the CNN would successfully map the measured instantaneous frequency to the nominal instantaneous frequency.

To develop the training dataset for our CNN, we use the B-IFM module to acquire numerous instantaneous frequencies. For our experiment, a distributed-feedback laser (DFB-LD, NEL NLK1C6DAAA) is used as a light source. The powers of pump and probe lightwaves injected into the fiber are around 23 and 20 dBm, respectively. The lower sideband of the SSBM is selected as the pump lightwave, and the carrier suppression is about 20 dB. The

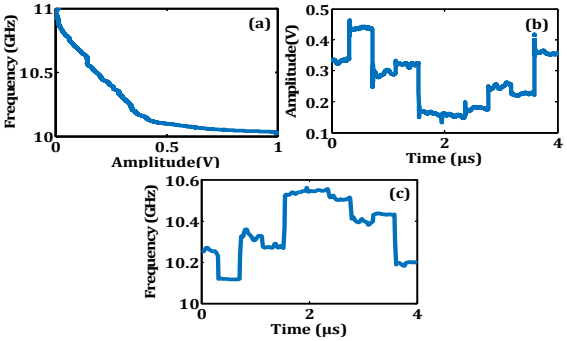

Fig. 2 (a) Measured ACF, (b) detected Brillouin gain, and (c) measured instantaneous frequency.

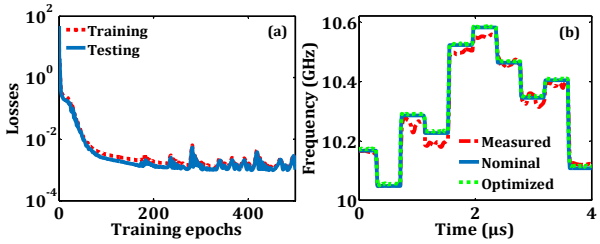

Fig. 3. (a) Training and testing loss curves. (b) Optimization result for a measured instantaneous frequency.

bandwidth of the PD is 300 MHz, while the optical power before the PD is −5 dBm. The sampling rate of the oscilloscope (Keysight, DSO- S 804A) is 2.5 GSa/s and. Its bandwidth is set to 200 MHz. The Brillouin frequency shift (BFS) of a 6.6-km-long DCF is 9.47 GHz. The nonlinear frequency sweeping signal ranges from 0.53 GHz to 1.53 GHz and the known LFM pulse varies from 10 GHz to 11 GHz. Figure 2 shows the experimental results of the B-IFM module for a Costas frequency modulated pulse. Within it, Fig. 2(a) displays the normalized amplitude comparison function (ACF) curve, while Fig. 2(b) shows its Brillouin gain normalized according to the ACF. By comparing Brillouin gain values with the ACF, we obtain the instantaneous frequencies as Fig. 2(c) shows.

An arbitrary waveform generator (AWG, Keysight M8152A) is used to produce 400 unknown broadband signals of various types, including LFM (up-chirp), LFM (down-chirp), NLFM, BFSK, and Costas frequency modulated signals. Eighty signals of each of these types were produced. The frequency range of these broadband signals is 10–11 GHz. In particular, the carrier frequencies and bandwidths are within 10–10.2 GHz and 0.3–1 GHz, respectively. The values of carrier frequency and bandwidth are randomly produced. The power and the duration of each signal are 13.01 dBm and 4 μs, respectively. Instantaneous frequency of NLFM is $f = f_c + \frac{B}{\tau^2} \times t^2$, where f_c is the carrier frequency, B is the bandwidth, τ is the duration, and t is time. The code element of BFSK is a 10-bit code: $C_{BFSK} = [1,0,1,1,0,0,1,0,1,1]$and that of the Costas modulated pulse is $C_{Costas} = [3,1,5,4,9,10,8,6,7,2]$.

In order to improve learning efficiency and reduce computational complexity of the training process, we perform an average operation for every 36 sample points. Consequently, the number of sample points reduces from 10000 to 278. In addition, we use the corresponding nominal instantaneous frequencies as network reference data. For each signal type, we randomly selected 75 measured instantaneous frequencies for the training dataset, and the left 5 for the testing dataset. Hence, the number of training datasets is 375, while that of the testing dataset is 25. We perform the normalization operation on all data.

We used an Adam Optimizer [16] as the minimization algorithm to train the CNN. The learning rate is 0.004. The regularized parameter of the L2 regularize is 0.0005. The training epochs were set to 2500. Figure 3(a) depicts that the training and testing losses converge to ~10-4 as the training epochs proceed. Figure (3b) shows the optimization result. The measured instantaneous frequency is input into the well-trained CNN, and the network outputs the optimized frequencies. The latency of this CNN-optimized B-IFM system is around ~0.3 ms, which is composed of three parts: the time for the probe lightwave running in the DCF one time, for digital processing, and for the optimization of the well-trained CNN. The training time of the CNN is about 3 h on a personal computer with an Intel(R) Core (TM) i7-8700 CPU.

The optimization effects of the CNN module in the testing dataset are illustrated in Fig. 4. The measured instantaneous frequencies differ from the corresponding nominal values. However, after CNN optimization, the outputted optimized instantaneous frequencies are considerably close to the nominal values. For each type of frequency modulation signals, we calculate $MAX_{average}$ and $RMS_{average}$ between the measured and nominal instantaneous frequencies and those between the optimized and nominal instantaneous frequencies based on the following formulas:

$$\boldsymbol{Max}_{\boldsymbol{average}} = \frac{1}{5}\sum_{i=1}^{5} Max_i, \quad \textbf{(2)}$$

$$\boldsymbol{RMS}_{\boldsymbol{average}} = \frac{1}{5}\sum_{i=1}^{5} RMS_i, \quad \textbf{(3)}$$

where $MAX_i$and $RMS_i$are the maximum and RMS error between the measured or optimized instantaneous frequency and the nominal one of the *ith* sample for each signal type, respectively. The calculation results are summarized in Table 1. Before optimization, $MAX_{average}$ and $RMS_{average}$ are up to 105.8 MHz and 57.0 MHz, respectively. In contrast, after CNN optimization, they reduce to less than 26.3 MHz and 15.5 MHz, respectively.

We remain the MZM in Fig. 1. biased at the quadrature point [17] of 4.30 volts and use the Costas frequency modulated signals within 10-11GHz to test the system sensitivity and dynamic range. Since the maximum voltage of the AWG we used is 1 volt, we deduce the maximum power to be 13.01 dBm according to the formula of $P=V^2/50\ \Omega$, where P is the power and V is the voltage. As Table2 shows, for the original B-IFM system, the system sensitivity is about 12.10 dBm for the 100-MHz frequency error. When the power is 7.82 dBm, after the CNN optimization, the frequency error is 43.5 MHz. Below 7.82 dBm, the measurement result of the original B-IFM can be regarded as wrong and we cannot collect dataset to train the CNN. Hence, by the optimization of the CNN, the system sensitivity is increased from 12.10 dBm to 7.82 dBm. We estimate the higher limit of power of the original B-IFM system under the assistant of an amplifier (CLN-1G18G-3025-S) and a stepping attenuator (KST-90). The result is around 29.01dBm for the 100-MHz frequency error. Therefore, the dynamic range of the CNN-optimized B-IFM is beyond 21.19 dB.

For our proposed CNN-optimized B-IFM system, the unknown signals that need to be measured should necessarily have similar features to those using which the CNN was trained, including modulation type, carrier frequency, power, and bandwidth. This is consistent with "No Free Lunch" theory [18] in machine learning.

Table 1. Comparison of $\boldsymbol{MAX}_{\boldsymbol{average}}$ and $\boldsymbol{RMS}_{\boldsymbol{average}}$ in MHz before and after optimization

	$MAX_{average}$		$RMS_{average}$	
	Measured	Optimized	Measured	Optimized
LFM (up-chirp)	103.3	**24.1**	57.0	**12.0**
LFM (down-chirp)	102.0	**17.9**	26.4	**10.2**
NLFM	103.5	**20.0**	52.1	**9.7**
BFSK	105.8	**26.3**	38.4	**15.5**
Costas	100.7	**18.9**	27.6	**8.4**

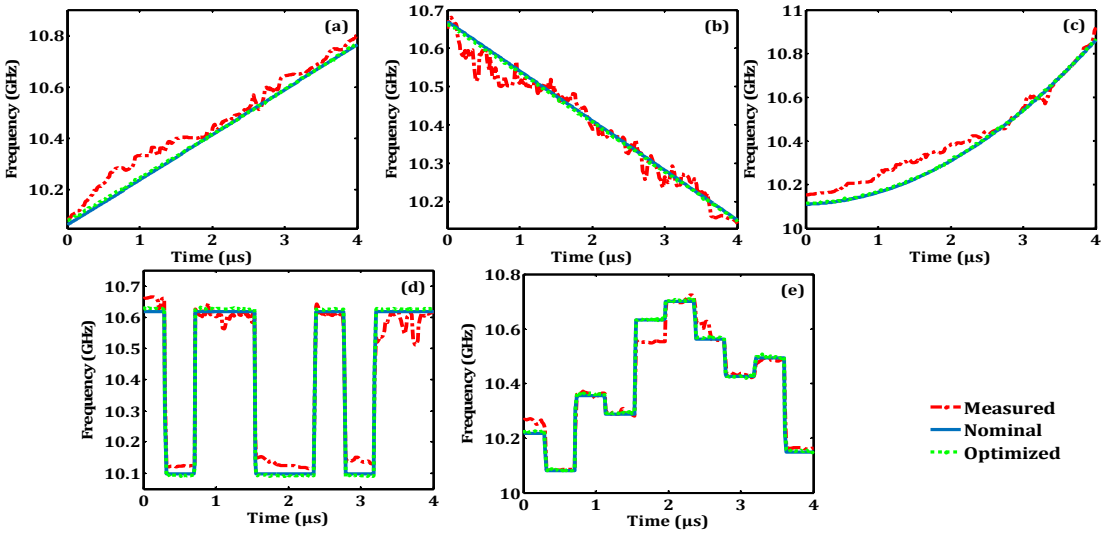

Fig. 4. Optimization effects for the testing dataset of the five different signal types. (a) LFM (up-chirp), (b) LFM (down-chirp), (c) NLFM, (d) BFSK, and (e) Costas modulated pulses. Red dashed curves: measured instantaneous frequencies; green dotted curves: optimized instantaneous frequencies; blue solid curves: nominal instantaneous frequencies.

Thus, we verified the feasibility and effectiveness of B-IFM performance improvements via deep learning by demonstrating the CNN-optimized performance of signals with the frequency range of 10–11 GHz for five types of frequency modulated signals. In fact, the B-IFM system could achieve a frequency resolution of 100 MHz with the 6 GHz instantaneous bandwidth at Ku band [4]. And other deep learning approaches could also be effective in optimizing the B-IFM. In future, we will attempt to achieve accurate B-IFM with more complicated signals that possess larger bandwidth, more complexed modulation, and combinations of one or more other signals, through various deep learning approaches, like CNNs, recurrent neural networks (RNNs), or fully connected neural networks (FNNs).

In conclusion, our CNN can optimize the B-IFM, improving the frequency accuracy, system sensitivity, and dynamic range. A trained CNN outputs the optimized instantaneous frequency when the instantaneous frequency of an unknown signal measured by the B-IFM module is input. The proposed CNN was trained and verified for five types of signals, i.e., LFM (up-chirp), LFM (down-chirp), NLFM, BFSK, and Costas frequency modulated signals. Under the power of 13.01 dBm, for the testing dataset used in our study, the average maximum and RMS errors between the optimized and nominal instantaneous frequencies are all less than 26.3 MHz and 15.5 MHz, respectively. After the CNN optimization, the system sensitivity is increased to 7.8 dBm and dynamic range is larger. The CNN-optimized B-IFM might enable accurate frequency detection of broadband electromagnetic signals in wide fields, such as radar and wireless communication.

Table 2. The measured frequency error at different power values of broadband microwave signal in a unit of MHz

	Power (dBm)				
	13.01	12.10	11.07	9.91	7.82
Original B-IFM	96.3	105.8	180.2	369.3	537.5
CNN-optimized B-IFM	11.7	----	----	----	43.5

Funding. National Natural Science Foundation of China (NSFC) (61822508, 61571292, 61535006).

REFERENCES

1. X. Long, W. Zou, and J. Chen, Opt. Express **25**, 2206 (2017).
2. H. Emami, M. Ashourian, and M. Ebnali-Heidari, J. Light. Technol. **32**, 4194 (2014).
3. J. Zhou, S. Fu, S. Aditya, P. P. Shum, and C. Lin, IEEE Photonics Technol. Lett. **21**, 1069 (2009).
4. X. Long, W. Zou, X. Li, G. Xin, and J. Chen, Opt. Lett., **8**, 2045 (2019).
5. Y. LeCun, Y. Bengio, and G. Hinton, Nature **521**, 436 (2015).
6. C. Arteaga and I. Marrero, Neural Netw. **46**, 299 (2013).
7. J. Tompson, A. Jain, Y. LeCun, and C. Bregler, Adv. Neural Inf. Process. Syst. **27**, 1799 (2014).
8. M. Anthimopoulos, S. Christodoulidis, L. Ebner, A. Christe, and S. Mougiakakou, IEEE T. Med. Imaging **35**, 1207 (2016).
9. R. Won, Nat. Photonics **12**, 571 (2018).
10. S. Xu, X. Zou, B. Ma, J. Chen, L. Yu, and W. Zou, Light Sci. & Appl. **8,** 66, (2019).
11. J. P. Salvestrini, L. Guilbert, M. Fontana, M. Abarkan, and S. Guille, J. Lightwave Technol. **29**, 1522 (2011).
12. C. Lin, J. Chen, S. Dai, P. Peng, and S. Chi, J. Lightwave Technol. **26**, 2449 (2008).
13. K. Tachibana, and K. Otsuka, *IEEE Society of Instrument and Control Engineers of Japan (SICE)* (2018), pp. 1029–1034.
14. M. E. Purbaya, N. A. Setiawan, and T. B. Adji, *International Conference on Information and Communications Technology (ICOIACT)* (2018), pp. 360-365.
15. K. Hornik, M. Stinchcombe, H. White, Neural Netw., **2**, 359 (1989).
16. D. P. Kingma and J. Ba, *International Conference on Learning Representations (ICLR)* (2015).
17. N. Sarkhosh, H. Emami, K. Ghorbani, L. Bui, and A. Mitchell, in IEEE MTT-S Int. Microw. Symp. Dig., Boston, MA, USA (2009), pp. 165–168.
18. H. Emami and M. Ashourian, IEEE Trans. Microw. Theory Techn., **62**, no. 10, pp. 2462–2470, Oct. 2014.

REFERENCES

1. X. Long, W. Zou, and J. Chen, "Broadband instantaneous frequency measurement based on stimulated Brillouin scattering," Opt. Express **25**(3), 2206-2214 (2017).
2. J. Zhou, S. Fu, S. Aditya, P. P. Shum, and C. Lin, "Instantaneous microwave frequency measurement using photonic technique," IEEE Photonics Technol. Lett. **21**(15), 1069–1071 (2009).
3. H. Emami, M. Ashourian, and M. Ebnali-Heidari, "Dynamically reconfigurable all optical frequency measurement system," J. Light. Technol. **32**(24), 4194–4200 (2014).
4. X. Long, W. Zou, X. Li, G. Xin, and J. Chen, "Brillouin instantaneous frequency measurement with arbitrary response for potential real-time implementation," Opt. Lett., **8**(44), 2045-2048, (2019).
5. Y. LeCun, Y. Bengio, and G. Hinton, "Deep learning," Nature **521**, 436-444 (2015).
6. C. Arteaga, and I. Marrero, "Approximation by neural networks with weights varying on a finite set of directions", Neural Netw., **46**, 299-305 (2013).
7. J. Tompson, A. Jain, Y. LeCun, and C. Bregler, "Joint training of a convolutional network and a graphical model for human pose estimation," Adv. Neural Inf. Process. Syst. **27**, 1799-1807 (2014).
8. M. Anthimopoulos, S. Christodoulidis, L. Ebner, A. Christe, and S. Mougiakakou, "Lung pattern classification for interstitial lung disease using a deep convolutional neural network," IEEE T. Med. Imaging **35**, 1207-1216 (2016).
9. R. Won, "Intelligent learning with light," Nat. Photonics **12**, 571–573 (2018).
10. S. Xu, X. Zou, B. Ma, J. Chen, L. Yu, and W. Zou, "Analog-to-digital conversion revolutionized by deep learning," Light Sci. & Appl. **8**, 66 (2019)
11. J. P. Salvestrini, L. Guilbert, M. Fontana, M. Abarkan, and S. Guille, "Analysis and Control of the DC Drift in LiNbO -Based Mach–Zehnder Modulators," J. Lightwave Technol. **29**, 1522 (2011).
12. C. Lin, J. Chen, S. Dai, P. Peng, and S. Chi, "Impact of nonlinear transfer function and imperfect splitting ratio of MZM on optical up-conversion employing double sideband with carrier suppression modulation," J. Lightwave Technol., **26**(15), 2449-2459 (2008).
13. K. Tachibana, and K. Otsuka, "Wind Prediction Performance of Complex Neural Network with ReLU Activation Function," *IEEE Society of Instrument and Control Engineers of Japan (SICE)*, 1029 – 1034 (2018).
14. M. E. Purbaya, N. A. Setiawan, andT. B. Adji, "Leaves Image Synthesis Using Generative Adversarial Networks with Regularization Improvement," *International Conference on Information and Communications Technology (ICOIACT)*, 360-365 (2018).
15. K. Hornik, M. Stinchcombe, H. White, "Multilayer feedforward networks are universal approximators," Neural Netw., **2**(5), 359-366 (1989).
16. D. P. Kingma, and J. Ba, "Adam: A Method for Stochastic Optimization," *International Conference on Learning Representations (ICLR)* (2015).
17. H. Emami and M. Ashourian, "Improved dynamic range microwave photonic instantaneous frequency measurement based on four-wave mixing," IEEE Trans. Microw. Theory Techn., **62**, no. 10, pp. 2462–2470, Oct. 2014.
18. D. H. Wolpert and W. G. Macready, No free lunch theorem for optimization, IEEE Trans. Evolutionary Computing **1**, 67-82 (1997).